ACS EARTH AND SPACE CHEMISTRY

Article

Cite This: ACS Earth Space Chem. XXXX, XXX, XXX−XXX

http://pubs.acs.org/journal/aesccq

Carbonate Adsorption to Ferrihydrite: Competitive Interaction with Phosphate for Use in Soil Systems

Juan C. Mendez* and Tjisse Hiemstra

Soil Chemistry and Chemical Soil Quality Group, Wageningen University, 6708 PB, Wageningen, The Netherlands

Supporting Information

ABSTRACT: Carbonate (CO_3) interacts with Fe-(hydr)-oxide nanoparticles, affecting the availability and geochemical cycle of other important oxyanions in nature. Here, we studied the carbonate−phosphate interaction in closed systems with freshly prepared ferrihydrite (Fh), using batch experiments that cover a wide range of pH values, ionic strength, and CO_3 and PO_4 concentrations. The surface speciation of CO_3 has been assessed by interpreting the ion competition with the Charge Distribution (CD) model, using CD coefficients derived from MO/DTF optimized geometries. Adsorption of CO_3 occurs predominately via formation of bidentate inner-sphere complexes, either $(\equiv FeO)_2CO$ or $(\equiv FeO)_2CO{\cdot\cdot}Na^+$. The latter complex is electrostatically promoted at high pH and in the presence of adsorbed PO_4. Additionally, a minor complex is present at high CO_3 loadings. The CD model, solely parametrized by measuring the pH-dependent PO_4 adsorption as a function of the CO_3 concentration, successfully predicts the CO_3 adsorption to Fh in single-ion systems. The adsorption affinity of CO_3 to Fh is higher than to goethite, particularly at high pH and CO_3 loadings due to the enhanced formation $(\equiv FeO)_2CO{\cdot\cdot}Na^+$. The PO_4 adsorption isotherm in 0.5 M $NaHCO_3$ can be well described, being relevant for assessing the reactive surface area of the natural oxide fraction with soil extractions and CD modeling. Additionally, we have evaluated the enhanced Fh solubility due to Fe(III)-CO_3 complex formation and resolved a new species ($Fe(CO_3)_2(OH)_2^{3-}(aq)$), which is dominant in closed systems at high pH. The measured solubility of our Fh agrees with the size-dependent solubility predicted using the surface Gibbs free energy of Fh.

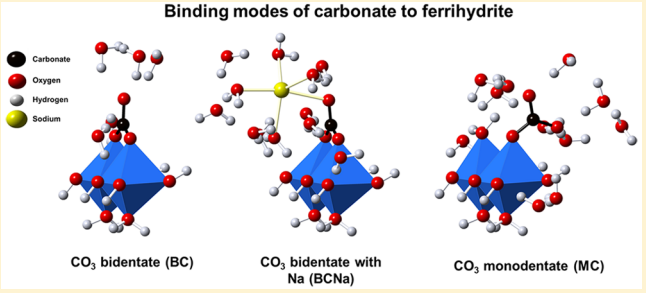

KEYWORDS: *ferrihydrite, goethite, nanoparticles, ion adsorption, surface complexation, competition, CD model, solubility*

1. INTRODUCTION

The adsorption of ions to the natural Fe-(hydr)oxides of soils is a key process that regulates the bioavailability, toxicity, and mobility of specific nutrients and contaminants in the environment.[1] Particularly, understanding the interaction between Fe-(hydr)oxide nanoparticles (FeNPs) and oxyanions such as phosphate (PO_4^{3-}), sulfate (SO_4^{2-}), silicate (SiO_4^{4-}), and arsenate (AsO_4^{3-}) is of great relevance as its behavior varies under a wide range of environmental conditions.[2−6] Moreover, recent developments in nanotechnology have shown promising results for the application of engineered FeNPs in a series of environmental and industrial cleanup applications, such as drinking and wastewater treatment.[7−9]

In relation to the ion adsorption capacity, ferrihydrite (Fh) is one of the most reactive FeNPs. The large reactivity of Fh is due to its high specific surface area (SSA ≥ 600 $m^2\ g^{-1}$) and high density of reactive surface groups.[10,11] Fh is ubiquitously present in terrestrial and aquatic systems[12,13] and, from the thermodynamic perspective, it is the most stable Fe-(hydr)-oxide at the nanometer scale.[14] Therefore, the study of the fundamental processes that regulate the interaction of ions with Fh is essential to understand and predict the adsorption behavior of these ions in a variety of systems.

Dissolved inorganic carbon, hereinafter called dissolved carbonate (CO_3), is another ubiquitous component in terrestrial and aquatic systems. The concentration of CO_3 in natural systems such as rivers and groundwater ranges over about 2 orders of magnitude (~0.1−10 mM).[15,16] An important property of CO_3 is its capacity to interact with the mineral surfaces of Fe-(hydr)oxides,[17,18] affecting the solid−solution partitioning of a whole suite of important ions in the environment,[19−28] including PO_4.[29,30]

From an environmental perspective, quantifying the CO_3−PO_4 interaction on the surfaces of the Fe-(hydr)oxides is important for understanding the reactivity of the natural oxide fraction. This aspect is essential for assessing the fate of nutrients and pollutants in the environment with Surface Complexation Modeling (SCM). The CO_3−PO_4 interaction has been previously used to assess the reactive surface area (RSA) of soil samples.[31] In that approach, the PO_4 buffer capacity of soils is measured by equilibrating the soil with a 0.5 M $NaHCO_3$ solution (pH = 8.5) at different soil-to-solution

Received: October 18, 2018
Revised: November 30, 2018
Accepted: December 2, 2018
Published: December 3, 2018

ratios. The resulting desorption isotherm has been interpreted with a SCM that was calibrated for the CO_3−PO_4 interaction with goethite (α-FeOOH). This material was chosen because of the existence of an internally consistent database with intrinsic adsorption constants. However, the application of this methodology to field samples revealed that the natural oxide fraction of top soils is dominated by nanoparticles ($d \sim 2-10$ nm) with a corresponding high specific surface area (SSA ∼ 200−1200 $m^2\ g^{-1}$). It suggests that Fh, rather than well-crystallized goethite, may be a better proxy for the natural oxide fraction in top soils.[31]

To date, no information is available about the competitive interaction of CO_3 and PO_4 at the surface of Fh. In addition, only a single data set is available in the literature with respect to CO_3 adsorption in monocomponent systems with Fh.[24] These data have been collected using ^{14}C dating, assuming no other source of CO_3 in the system than added. Moreover, the adsorption was only studied at very low concentrations of CO_3 (μM level), which are much below the natural concentration range. The lack of reliable information about the adsorption of CO_3 to Fh, in systems with and without PO_4 ion competition, underlines the scientific and practical relevance of the present research. Our study has a wide perspective as CO_3 is omnipresent in nature and will interfere in many geochemical processes, as mentioned above.[6,19−30]

In the present study, our main objective is to measure the interaction of CO_3 with the surfaces of freshly prepared Fh in a series of batch experiments that cover a wide range of chemical conditions. Since measuring the CO_3 adsorption is challenging from an analytical perspective, a significant part of our experimental study will refer to the assessment of the interaction of CO_3 with PO_4 as a function of pH (∼7−12), ionic strength (0.05−0.5 M), total CO_3 concentration (4 mM−0.5 M), and PO_4 loading (0.68−1.48 μmol m^{-2}). The interaction of CO_3 with Fh will be parametrized by measuring the competitive effect of this anion in the adsorption of PO_4. A similar approach has been used successfully to derive the CO_3 interaction with goethite.[29]

The charge distribution (CD) model[32] will be used to interpret the collected competition data, in combination with state-of-the-art knowledge about the mineral and surface structure of Fh.[10,11,33] To limit the number of adjustable parameters to one per complex (i.e., log K), the CD coefficients will be derived with a bond valence analysis[34,35] of the optimized geometry of the CO_3 surface complexes, obtained with molecular orbital (MO) calculations, applying density functional theory (DFT).

Since Fh is a nanoparticle *pur sang*, most of its properties are size dependent. The molar mass (M_{nano}) will increase with smaller particle size[11] due to the change of the chemical composition $FeO_{1.4}(OH)_{0.2}{\cdot}nH_2O$ by the presence of surface groups, giving rise to a size dependent amount of chemisorbed water (nH_2O). This will also lead to a decrease of the mass density (ρ) as this chemisorbed water does contribute more to the volume of the particle than to its mass.[36] These changes in M_{nano} and ρ will affect the relation between the specific surface area of Fh and its particle size. The size will also change the capacitance values of the Stern layers used in the electrostatic part of the model.[36] The size-dependence of the above properties will be considered in our modeling, using a consistent set of equations.[36,37]

In addition to the CO_3−PO_4 competition data, the CO_3−Fh interaction will be studied for single-ion systems. The CD model, parametrized for the PO_4−CO_3 interaction, will be applied to compare the experimental adsorption of CO_3 with the model predictions for single-ion systems. With the derived adsorption parameters, we will evaluate the surface speciation of CO_3 in Fh systems as a function of solution conditions such as pH, ionic strength, and anion concentrations. In the last part of the paper, we will compare the CO_3 interaction of Fh and goethite and show that the significant differences between both materials can be understood from the difference of the interaction of Na^+ with adsorbed CO_3. This will lead to a strong difference of the competitive behavior of CO_3 with PO_4 bound by either Fh or goethite. It will have important implications for assessing the RSA of field soil samples, as we will discuss briefly.

2. EXPERIMENTAL SECTION

For all the adsorption experiments, ultrapure water (18.2 MΩ cm at 25 °C, <1 ppb TOC) and chemical reactants of analytical grade were used to prepare the stock solutions and the Fh suspensions. Contact between solutions and air was largely avoided to reduce the interference of atmospheric $CO_{2(g)}$ during the adsorption experiments.

2.1. Ferrihydrite Synthesis. Fh suspensions were prepared by fast neutralizing with 0.02 M NaOH a solution of ∼3.7 mM of $Fe(NO_3)_3$ dissolved in 0.010 M HNO_3. Freshly prepared acid and base solutions were always used. The neutralization was initially done at a rate of ∼200 mL NaOH min^{-1} until a pH of ∼3.2 was reached. More NaOH solution was subsequently added in ∼5 mL increments until the suspension reached a final stable pH (over 15 min) of ∼8.2 for the binary CO_3−PO_4 adsorption experiments, or pH ∼6.0 for the CO_3 adsorption experiments in monocomponent systems. The Fh suspensions were centrifuged at 3500*g* for 45 min, the supernatant was carefully removed, and the settled Fh particles were resuspended in a 0.01 M $NaNO_3$ solution. The Fh suspensions were aged at 20 °C for 4 h since formation before starting the CO_3−PO_4 competition experiments. Due to the relatively low level of added CO_3, the results of the adsorption experiments of CO_3 in single-ion systems may be particularly sensitive to interference of atmospheric $CO_{2(g)}$. Therefore, the Fh suspensions used in these systems were first acidified to pH ∼5.5 and purged during 24 h with moist purified $N_{2(g)}$ before starting the adsorption experiments. The total Fe concentration ($Fe_{[T]}$) of each Fh suspension was measured by ICP-OES in a matrix of 0.8 M H_2SO_4. The $Fe_{[T]}$ was typically 19.3 ± 0.7 mM, which is equivalent to 1.90 ± 0.07 g Fh L^{-1} (for a mean Fh molar mass of M_{nano} = 97.6 g Fh mol^{-1} Fe). The specific surface area (*SSA* in $m^2\ g^{-1}$) of each Fh suspension was assessed independently by using PO_4 as probe ion.[37] The values of $Fe_{[T]}$, *SSA*, and M_{nano} corresponding to each Fh preparation are presented in Table S-1 of the Supporting Information (SI).

2.2. Competitive Adsorption Carbonate-Phosphate. The competitive interaction of CO_3 with PO_4 was experimentally evaluated by determining the adsorption edges of PO_4 in a series of closed Fh systems with different concentrations of both oxyanions. Each individual system was prepared in 50 mL polypropylene tubes and contained a total volume of 40.0 mL. First, the required volume of ultrapure water and 4 M $NaNO_3$ solution was added into the tubes according to the intended final volume and background electrolyte level. Next, aliquots of 10.0 or 15.0 mL of the freshly prepared Fh were pipetted into the tubes and the pH of

DOI: 10.1021/acsearthspacechem.8b00160
ACS Earth Space Chem. XXXX, XXX, XXX−XXX

the suspensions was adjusted by adding acid (HNO_3) or base (NaOH) solutions, leading to pH ~6.5−11. Adsorption systems with pH values below 6.5 were not prepared to prevent the escape of HCO_3^- to the atmosphere as $CO_{2(g)}$. Finally, volumes of the stock solution of NaH_2PO_4 (0.010 M) and $NaHCO_3$ (0.10 or 1.0 M) were pipetted into the tubes. The $NaHCO_3$ solutions were freshly prepared before each experiment. Total PO_4 concentrations ($PO_{4[T]}$) of 0.25 and 0.50 mM were used in the systems with a low Fh content, whereas $PO_{4[T]}$ of 0.50 and 0.75 mM were used in the systems with a high Fh content. These combinations resulted in systems with a total PO_4 loading ($PO_{4(T)}$) equivalent to 0.68, 1.07, and 1.48 μmol m^{-2}. The total CO_3 concentrations ($CO_{3[T]}$) varied between 4.0 mM and 0.50 M. Most of the experiments were performed at a constant ionic strength of I = 0.50 M. Additional experiments were done at I = 0.050 and 0.10 M for evaluating the effect of different Na^+ levels on the competitive interaction of CO_3−PO_4. A summary of the chemical conditions for each experimental series is presented in Table S-1 of the Supporting Information.

The thus-prepared CO_3−PO_4 systems with Fh were constantly shaken (120 strokes min^{-1}) in a conditioned room at 20 °C. After 20 h of equilibration, the suspensions were centrifuged at 3500g for 20 min to separate the Fh nanoparticles and the liquid phase. The equilibrium pH of the solution was measured with a glass electrode, and immediately after this, an aliquot of 10 mL was taken from the supernatant for chemical analysis. This aliquot was filtered through a 0.45 μm filter and acidified with HNO_3 to analyze the total concentration of P in solution by either ICP-OES or ICP-MS, depending on the final concentration of P. The concentration of Fe was also measured in the supernatant of a selected number of samples to test if significant dissolution of Fh occurred during the adsorption experiments, due to the formation of aqueous Fe(III)-CO_3 complexes.[38]

2.3. Carbonate Adsorption in Monocomponent Systems. The adsorption of CO_3 in monocomponent systems with Fh was experimentally evaluated following a similar procedure than used for the binary CO_3−PO_4 systems. The pH of the adsorption systems ranged from ~6.5 to ~10.5, and the ionic strength was kept constant at I = 0.10 $NaNO_3$. Aliquots of 10, 20, or 30 mL of Fh suspension, aged for 24 h, were pipetted into the systems with a final solution volume of 40 mL. The $CO_{3[T]}$ was 1 mM, which was added using a freshly prepared 0.010 M $NaHCO_3$ stock solution. The gas-to-solution ratio of the systems was 0.25 mL mL^{-1}, which was used in the model calculations to account for the distribution of the total added CO_3 over the gas and liquid phases. The samples were equilibrated for 20 h at 20 °C, and after centrifugation, a volume of 10 mL of solution was rapidly taken for analysis of the CO_3 concentration. The equilibrium pH was immediately measured in the remaining supernatant. The CO_3 concentration in solution was measured with a TOC analyzer, which converts the dissolved inorganic carbon into $CO_{2(g)}$ by means of an internal acidification step. The concentration of produced $CO_{2(g)}$ is then measured with an IR detector. Internal standard solutions with known concentrations of total dissolved CO_3 were also analyzed to verify the accuracy of our measurements. At every moment, maximum care was taken to minimize the escape/intrusion of $CO_{2(g)}$ to/from the atmosphere.

2.4. CD Modeling and MO/DFT Calculations. The interaction between CO_3 and PO_4 at the mineral−solution interface of Fh has been described using the charge distribution (CD) model[32] in combination with the extended Stern layer model[39] that describes the compact part of the electrical double layer (EDL). In this electrostatic model, we have accounted for the effect of the nanosized spherical particles on the capacitance values (C_1 and C_2) of the inner and outer Stern layers, in relation to the capacitance values of a flat plane.[36] The types of sites and the corresponding site densities have been derived with a surface structural analysis of Fh[37] based on recent insights into the mineral and surface structure of this Fe-(hydr)oxide material.[10,11,33] Primary charge reactions have been described according to Hiemstra.[5] CD model parameters for describing the adsorption of PO_4 to Fh were taken from Hiemstra and Zhao,[37] whereas the parameters for CO_3 have been derived in the present study from modeling the competition experiments with PO_4. CD modeling was done with the software Ecosat,[40] version 4.9. The adsorption parameters for CO_3 were optimized using the program FIT,[41] version 2.581. The entire set of solution speciation reactions and primary charge reactions used in the modeling are presented respectively in Tables S-2 and S-3 given in the Supporting Information.

The geometries of the hydrated CO_3 complexes were optimized with molecular orbital (MO) calculations, using the Spartan14 parallel of Wavefunction, Inc. Density functional theory (DFT) was applied, using a range of functionals (BP86, B3LYP, EDF1, EDF2, BLYP, ωP97X-D). For the geometries optimization, we have used $(H_2O)_2Fe_2(OH)_6$ as template with fixed atomic positions[42] to which a hydrated moiety with CO_3^{2-}, HCO_3^-, or $NaCO_3^-$ was attached to form an inner-sphere complex that was allowed to freely relax. The average O−C bond lengths obtained with the different DFT functionals were interpreted with the Brown valence concept.[34,35] The resulting charge distribution coefficients have been corrected for the electrostatic contribution of water dipole orientation.[39]

3. RESULTS AND DISCUSSION

3.1. Dissolution of Ferrihydrite in Carbonate Media. Carbonate may significantly increase the solubility of Fe-(hydr)oxides[38,43,44] by forming aqueous Fe(III)-CO_3 complexes, particularly above neutral pH. As this may have influence on our interpretation of the CO_3−PO_4 adsorption experiments, we have first evaluated the solubility of Fh in a number of binary CO_3−PO_4 adsorption systems by measuring the concentration of Fe in the supernatant of these systems (Figure 1).

According to Grivé et al.,[38] two aqueous Fe(III)-CO_3 complexes may form in carbonate solutions, i.e. a neutral $FeOHCO_3^0$ complex that dominates the Fe(III) solution speciation at pH ~4−7 and a $Fe(CO_3)_3^{3-}$ complex that controls the Fe(III) speciation above pH 7. Formation of the latter species leads to a significant increase of the solubility of Fe-(hydr)oxides in open systems with high partial CO_2 pressures (Figure S-2). However, such partial pressures are not present in our closed systems because the total concentration of CO_3 remains constant with pH, in contrast to the open systems used by Grivé et al.[38] For the latter system, one may calculate the solubility of Fh as a function of pH, using the above given Fe(III)-CO_3 complexes. Representing Fh as $Fe(OH)_3(s)$, the formation reactions of these Fe(III)-CO_3 complexes can be given as

DOI: 10.1021/acsearthspacechem.8b00160
ACS Earth Space Chem. XXXX, XXX, XXX−XXX

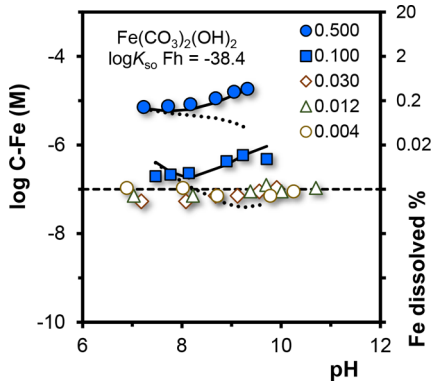

Figure 1. Logarithm of the experimental Fe concentrations (symbols) in the supernatants (left *y*-axis) and percentages of dissolved Fh (right *y*-axis) measured in our binary CO_3−PO_4−Fh systems as a function of pH for different $CO_{3[T]}$ with a fixed total concentration of Fe (4.9 mM) and PO_4 (0.25 mM) at a constant ionic strength (I = 0.5 M). Only the systems with 0.50 and 0.10 M $CO_{3[T]}$ have Fe concentrations that are clearly above the detection limit (dashed line) of our ICP-MS measurements. This detection limit is relatively high due to the very high electrolyte concentration that requires dilution. Dotted lines are model predictions including only the Fe(III)-CO_3 complexes proposed by Grivé et al.,[38] whereas the solid lines are model predictions using additionally $Fe(CO_3)_2(OH)_2^{3-}(aq)$ (See text). The solubility of our Fh was found to be log Q = log(Fe^{3+}) + 3 log(OH^-) = −38.4 ± 0.1, which is in line with the solubility calculated for Fh with a mean particle size of ∼2.2 nm and a specific surface area of 765 $m^2\ g^{-1}$ (logQ_{so} = −38.2 ± 0.2) applying the Ostwald equation with a surface Gibbs free energy of 0.186 ± 0.01 J m^{-2} and an intrinsic (bulk) solubility of log K_{so} = −40.6 ± 0.1 as described elsewhere.[14]

$$Fe(OH)_3(s) + HCO_3^-(aq) + H^+(aq) \Leftrightarrow FeOHCO_3^0(aq) + 2H_2O(l) \quad (1)$$

$$Fe(OH)_3(s) + 3HCO_3^-(aq) \Leftrightarrow Fe(CO_3)_3^{3-}(aq) + 3H_2O(l) \quad (2)$$

For solutions with a constant concentration of HCO_3^-, the overall solubility of Fh will be pH-independent, if the solution speciation of Fe is dominated by $Fe(CO_3)_3^{3-}(aq)$. As $HCO_3^-(aq)$ gradually transforms into $CO_3^{2-}(aq)$ at high pH, the solubility of Fh is predicted to decrease (dotted lines in Figure 1), whereas our data show an opposite trend with pH. The difference can be explained by the formation of an additional Fe(III)-CO_3 species. Our experimental data for the dissolved Fe concentrations can be described by assuming the formation of an extra Fe(III)-CO_3 complex, according to the reaction:

$$Fe(OH)_3(s) + 2HCO_3^-(aq) \Leftrightarrow Fe(CO_3)_2(OH)_2^{3-}(aq) + H^+(aq) + 1H_2O(l) \quad (3)$$

The log K values of reactions 1−3 are respectively log K = 24.86 ± 0.09, 24.86 ± 0.09, and 31.71 ± 0.13. Details on deriving these constants as well as the solubility product of our Fh material can be found in Appendix 5 of the SI.

In Figure 1, the right *y*-axis gives the fraction of the total Fe that is dissolved in our systems. For the systems with a $CO_{3[T]}$ of 0.50 M, less than ∼0.5% of the total Fe is dissolved at the highest pH. This implies that the effect of CO_3 on the dissolution of Fh is negligible under our experimental conditions, as nearly 100% of the total Fe in the systems remains part of the solid phase.

3.2. Interaction Carbonate-Phosphate in Ferrihydrite Systems. *3.2.1. Influence of pH and Carbonate Concentration.* Figure 2 presents the adsorption edges of PO_4 to Fh for systems with different $CO_{3[T]}$ at two levels of $PO_{4(T)}$ equivalent to 0.68 (a) and 1.07 (b) μmol m^{-2}. The background Na^+ concentration was kept constant at 0.50 M by adding appropriate amounts of $NaNO_3$. A series of observations can be made focusing on these data. First, with increase of $CO_{3[T]}$, the PO_4 adsorption decreases. This illustrates the competition between both ions for the same binding sites at the surfaces of Fh. Second, the percentage of adsorbed PO_4 decreases when the solution pH increases. This pH-dependency is characteristic for oxyanions in general (PO_4^{3-}, AsO_4^{3-}, SO_4^{2-}) binding to the surfaces of Fe-(hydr)oxides.[45−47] With increase of pH, the protonated singly (≡$FeOH_2^{+0.5}$) and triply (≡$Fe_3OH^{+0.5}$) coordinated surface groups will gradually release protons. This will lead to a decrease of the electrostatic surface potential and, consequently, to less attraction of the negatively charged PO_4 ions by the surface.

Additionally, the adsorption of PO_4 to Fh does not decrease proportionally to the increase of the $CO_{3[T]}$ (Figure 2). This nonproportional effect is related to the higher affinity of PO_4 for the adsorption to Fh, in comparison with CO_3. A quite high

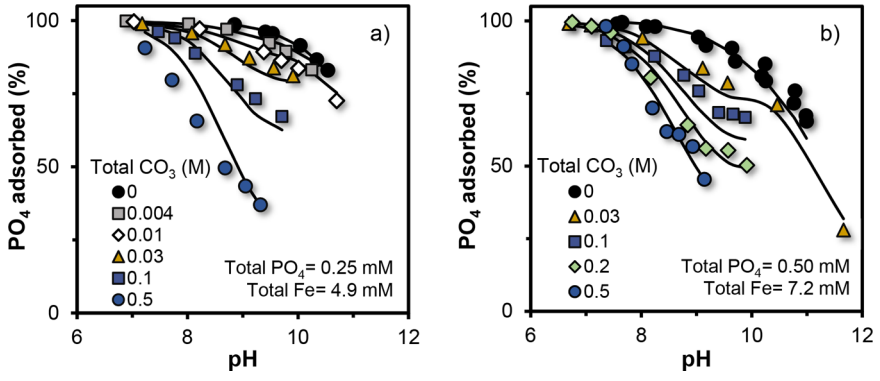

Figure 2. Adsorption edges of the competitive PO_4 binding to Fh in closed CO_3 systems at constant ionic strength of 0.50 M created by adding additionally $NaNO_3$. The symbols are experimental results, and the lines are CD model calculations applying the parameter set of Table 1. The zero-carbonate system has been used to derive the specific surface area of Fh, being for system (a) 765 and (b) 672 $m^2\ g^{-1}$ at a molar mass of respectively M_{nano} = 98.76 and 96.33 g mol^{-1} Fe. The initial PO_4 loadings are equivalent to 0.68 (a) and 1.07 (b) μmol m^{-2}.

DOI: 10.1021/acsearthspacechem.8b00160
ACS Earth Space Chem. XXXX, XXX, XXX−XXX

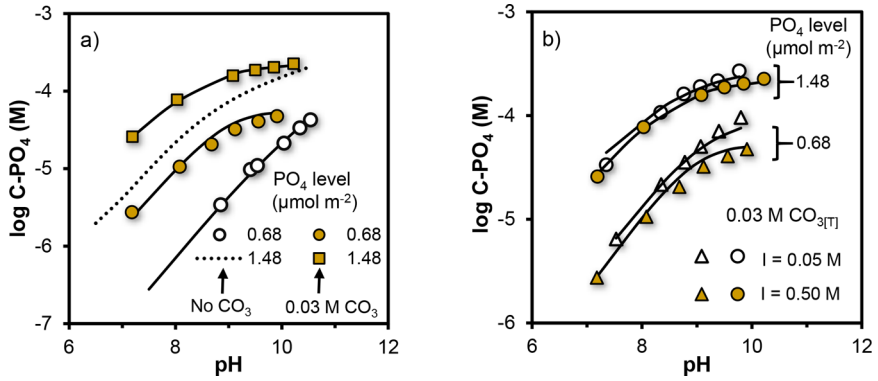

Figure 3. Logarithm of the equilibrium concentration of PO_4 as a function of pH in closed systems with Fh. Symbols are experimental results, and lines are CD model calculations using the parameter set of Table 1. The total Fe content was 4.5 mM for all the series, except for the colored triangle series in panel b, whose total Fe concentration was 4.9 mM. The calibrated specific surface area of the Fh suspensions used here was SSA = 765 $m^2\ g^{-1}$ at a molar mass of M_{nano} = 98.76 g mol^{-1} Fe. Panel a shows the effect of the addition of 0.03 M CO_3 (colored symbols) on the equilibrium PO_4 concentration for systems with two levels of $PO_{4(T)}$ (0.68 and 1.48 μmol $PO_4\ m^{-2}$). As reference, the equilibrium concentration of PO_4 in monocomponent systems has been measured and/or modeled (open symbols and dotted line). All data correspond to systems with an ionic strength of 0.5 M, made by adding additionally $NaNO_3$. Panel b presents the effect of the ionic strength (0.05 M for open symbols, 0.5 M for colored symbols) on the equilibrium PO_4 concentration for systems with a total $CO_{3[T]}$ = 0.03 M for two initial PO_4 loadings, as given.

concentration of CO_3 ions is needed before the adsorption of PO_4 to Fh is significantly suppressed. The competitive effect of CO_3 on the adsorption of PO_4 depends on the relative concentration of both ions in solution ($[PO_4]/[PO_4 + CO_3]$).

The relatively high affinity of PO_4 for binding to Fh can be depicted by constructing a normalized adsorption isotherm for binary CO_3–PO_4 systems. In this isotherm, the amount of adsorbed PO_4 as well as its solution concentration are presented on a relative scale (0–100%) with respect to the total amount adsorbed and total solution concentration of oxyanions ($[PO_4 + CO_3]$). The constructed isotherm (Figure S-4) shows that only a small fraction of dissolved PO_4 is needed to dominate the oxyanion adsorption onto Fh. This is very different for the adsorption of PO_4 in binary systems with a stronger competitor, as for instance AsO_4, where the normalized adsorption isotherm is much closer to a 1:1 line, as shown in Figure S-4 of the Supporting Information.

3.2.2. Influence of Phosphate Loading and Electrolyte Concentration. Figure 3a shows the equilibrium concentration of PO_4 in solution as a function of pH for systems that differ in surface loading with PO_4 (0.68 and 1.48 μmol m^{-2}) in the presence and absence of CO_3. Due to the competition with CO_3, the equilibrium concentration of PO_4 is higher in the systems with 0.03 M CO_3 in comparison to the corresponding PO_4 monocomponent systems. However, for a given pH, the extent of the CO_3 effect depends on the PO_4 level in the system. Addition of 0.03 M $CO_{3[T]}$ leads to a larger increase of the PO_4 concentration in the systems with the lower initial PO_4 loading.

Figure 3a also shows that CO_3 enhances the equilibrium concentration of PO_4 more at a lower pH. This is related to the pH dependency of the CO_3 adsorption, reaching a maximum near pH ~ 7, as we will show later in section 3.4.1. This has also been found for goethite[16,25] and matches qualitatively also with other data obtained for goethite using the same experimental approach.[29]

In Figure 3b, the effect of the ionic strength on the competitive interaction between CO_3 and PO_4 is shown. In general, a rather small effect of the ionic strength is observed, which is consistent with the formation of predominantly inner-sphere surface complexes for PO_4.[45,48−50] The largest differences are found at high pH and relatively low loading with PO_4.

The increase of the PO_4 adsorption with increase of ionic strength can be understood from a better screening of the repulsive interface charge at a higher ionic strength. The trend observed in Figure 3b agrees with the ionic strength dependency of the specific adsorption of anions in general as reported for monocomponent systems with Fh.[37,45,48] The adsorption of CO_3 contributes also to this trend as discussed in section 3.3.2.

3.3. Surface Complexation Modeling. In this section, we will explore the main mechanisms of the CO_3 adsorption to Fh by interpreting the results of the competitive CO_3–PO_4 adsorption experiments with the CD model.[32] A similar approach was successfully applied previously by Rahnemaie et al.[29] for describing the adsorption of CO_3 onto goethite.

3.3.1. Surface Structure of Ferrihydrite. Presently, we will apply the multisite ion adsorption model recently developed for Fh.[37] A surface structural analysis[37] reveals the presence of two types of reactive surface groups at the surface of Fh, namely singly ($\equiv FeOH^{-1/2}$) and the triply ($\equiv Fe_3O^{-1/2}$) coordinated groups. The singly coordinated groups are dominantly present having a total site density of 5.8 ± 0.3 nm^{-2} or 9.6 μmol m^{-2}. Based on the surface structure, two types of singly coordinated groups are defined: those that only allow the formation of monodentate surface complexes ($\equiv FeOH(a)^{-1/2}$) and those that in addition allow the formation of binuclear bidentate surfaces complexes ($\equiv FeOH(b)^{-1/2}$) with e.g. PO_4 and AsO_4 ions.[37] The site densities of these $\equiv FeOH(a)^{-1/2}$ and $\equiv FeOH(b)^{-1/2}$ groups are 3.0 ± 0.6 and 2.8 ± 0.6 nm^{-2}, respectively. The triply coordinated groups ($\equiv Fe_3O^{-1/2}$) do not participate directly in the ligand exchange reactions with oxyanions, but they contribute to the development of primary surface charge. The value for the effective site density of the $\equiv Fe_3O^{-1/2}$ groups (1.4 ± 0.5 nm^{-2}) has been derived by fitting PO_4 adsorption data to Fh.[37]

In the model, the proton affinity of both singly and triply coordinated groups has been set equal to the value of the point of zero charge (PZC) of Fh, according to

DOI: 10.1021/acsearthspacechem.8b00160
ACS Earth Space Chem. XXXX, XXX, XXX–XXX

$$\equiv FeOH^{-0.5} + H^+ \Leftrightarrow \equiv FeOH_2^{+0.5} \quad \log K_H = PZC = 8.1 \tag{4}$$

$$\equiv Fe_3O^{-0.5} + H^+ \Leftrightarrow \equiv Fe_3OH^{+0.5} \quad \log K_H = PZC = 8.1 \tag{5}$$

The above surface groups may also react with the background electrolyte ions (i.e., Na^+, NO_3^-) forming ion pairs. For reasons of consistency, we will rely on the set of adsorption parameters recently published by Hiemstra and Zhao[37] to describe the PO_4 adsorption to Fh.

3.3.2. Carbonate Surface Complexes. Structural information about surface complexes obtained with *in situ* spectroscopy studies is useful to formulate, within the CD model approach, a set of reactions that realistically reflect the molecular picture of the adsorption mechanisms. For CO_3, the surface speciation at the mineral−solution interface of metal-(hydr)oxides has been analyzed in several *in situ* spectroscopy studies.

Attenuated total reflectance-Fournier transformed infrared (ATR-FTIR) spectra have been interpreted previously as evidence for the dominant formation of inner-sphere monodentate CO_3 complexes at the surfaces of goethite.[51−53] The basis of this interpretation was the extent of peak splitting of the ν_3 band ($\Delta\nu_3$) of the O−C−O asymmetric stretching frequency, taking as a reference the $\Delta\nu_3$ value (80−137 cm^{-1}) for the formation of inner-sphere monodentate Co(III)-carbonato complexes in solution.[54] A critical evaluation by Hiemstra et al.,[55] combined with interpreting the charge distribution of the CO_3 surface species with SCM, suggested the dominant formation of inner-sphere bidentate complexes of CO_3 adsorbed to goethite. Bargar et al.[56] characterized the adsorption of CO_3 onto the hematite surface at various values of pH and ionic strength with ATR-FTIR spectroscopy and vibrational frequency calculations. The formation of an inner-sphere bidentate complex dominated the adsorption of CO_3 to hematite, especially at a high background electrolyte concentration (i.e., 0.1 M NaCl), whereas outer-sphere complexes may be relevant at a low pH and a low ionic strength. Kubicki et al.[57] applied MO/DFT calculations on molecular clusters to model the IR vibrational frequencies of the surface complex structures for a series of oxyanions (i.e., CO_3^{2-}, PO_4^{3-}, SO_4^{2-}, AsO_4^{3-}). A good agreement was found between the MO/DFT derived frequencies of a hydrated CO_3 bidentate complex and the experimental frequencies reported by Bargar et al.[56]

For Fh, recent evidence obtained with *in situ* ATR-FTIR spectroscopy and DFT calculations also suggests the formation of inner-sphere bidentate complex as one of the main adsorption mechanisms for CO_3 under atmospheric moisture conditions.[17] Therefore, we will first consider in our modeling the formation of a binuclear bidentate carbonate complex (BC) with ligand exchange according to

$$2\equiv FeOH(b)^{-0.5} + 2H^+(aq) + CO_3^{2-}(aq) \Leftrightarrow \equiv(FeO)_2^{-1+\Delta z_0}CO^{\Delta z_1} + 2H_2O(l) \quad \log K_{BC} \tag{6}$$

in which Δz_0 and Δz_1 are the charge attributed to the surface and inner Stern plane by the adsorbed ions ($\Delta z_0 + \Delta z_1 = 0$).

Solely considering this BC complex in the modeling provides a good description of the experimental PO_4 adsorption data for the series with $CO_{3[T]}$ levels below 0.03 M. However, the quality of fitting the entire experimental data set was rather poor (R^2 = 0.85, n = 146). The pH-dependency of the PO_4 adsorption to Fh was underestimated at the higher values of $CO_{3[T]}$, especially in the systems with the largest amount of added PO_4 (i.e., 1.07 and 1.48 μmol m^{-2}). Additionally, the effect of ionic strength on the PO_4−CO_3 competition was not well described.

In solution, Na^+ and CO_3^{2-} ions may interact forming relatively weak, yet important, ion pairs.[58,59] A similar interaction may occur at solid−solution interfaces. For a subset of data (n = 58), comprising only the adsorption series with $CO_{3[T]}$ of 0.03 and 0.1 M at three ionic strength levels (I = 0.05, 0.1, or 0.5 M), good description (R^2= 0.97) was found if ternary complex was included. The formation of a binuclear bidentate complex of CO_3 interacting with a Na^+ ion (BCNa) has been suggested previously for goethite[29,51] and can be formulated as

$$2\equiv FeOH(b)^{-0.5} + 2H^+(aq) + CO_3^{2-}(aq) + Na^+(aq) \Leftrightarrow \equiv(FeO)_2^{-1+\Delta z_0}CO\cdots Na^{+1+\Delta z_1} + 2H_2O(l) \quad \log K_{BCNa} \tag{7}$$

Modeling the results of our CO_3−PO_4 competition experiments suggests an attribution of the full Na^+ charge to the 1-plane of the Stern layer (section 3.3.3). It does not necessarily imply that Na^+ forms an inner-sphere complex with the outer O-ligand of the adsorbed CO_3. According to Bargar et al.,[56] a mechanism of $NaCO_3$ inner-sphere complexation is less likely, based on MO/DFT calculations comparing the experimental and calculated vibrational frequencies of CO_3 adsorbed to hematite. If the Na^+ ion of our resolved BCNa complex binds as a $Na\cdots CO_3$ ion pair, the Na^+ ion may search for the interfacial location that allows the strongest electrostatic attraction, which will be the 1-plane as the electric potential of the inner Stern plane is most negative in our PO_4−CO_3 systems.

By using two CO_3 inner-sphere complexes, a substantial part of our experimental data set can be well described. However, the adsorption of PO_4 to Fh is slightly overpredicted by the model in our systems with the highest $CO_{3[T]}$ levels (0.2 and 0.5 M); that is, the competitive effect of CO_3 is still insufficiently predicted by the model (R^2 = 0.90, n = 146). It is possible that an additional CO_3 surface complex contributes to the CO_3−PO_4 interaction. To explore the possibilities, we have defined additionally the formation of a monodentate carbonate (MC) complex according to

$$\equiv FeOH^{-0.5} + H^+(aq) + CO_3^{2-}(aq) \Leftrightarrow \equiv FeO^{-0.5+\Delta z_0}CO_2^{\Delta z_1} + 1H_2O(l) \quad \log K_{MC} \tag{8}$$

Note that the MC complex can be formed by reacting with both types of $\equiv FeOH^{-1/2}$ groups ($(\equiv FeOH(a)^{-1/2}$ as well as $\equiv FeOH(b)^{-1/2}$). For the surface complex in eq 8, we searched for the charge distribution by free fitting of the CD coefficients, resulting in Δz_0 = 0.26 ± 0.08 and Δz_1 = −1.26 ± 0.08 v.u. The obtained charge distribution shows that about 2/3 of the charge of the divalent CO_3^{2-} ion is present at the Stern plane and about 1/3 is at the surface. According to the Pauling bond valence concept, this can be interpreted as the formation of a monodentate inner-sphere complex having one O-ligand common with the Fe in the surface while both other O-ligands are outside the surface. The values for the CD coefficients found by fitting are in good agreement with the ones found by optimizing the geometry of that complex with

DOI: 10.1021/acsearthspacechem.8b00160
ACS Earth Space Chem. XXXX, XXX, XXX−XXX

Table 1. Table Defining the Surface Species, CD Values, and log *K* for the Adsorption Reactions of CO_3 and PO_4 to Ferrihydrite[a]

Surface species	ID[b]	≡FeOH(a)$^{-0.5}$[c]	≡FeOH(b)$^{-0.5}$[c]	≡Fe3O$^{-0.5}$	Δz_0	Δz_1	Δz_2	H^+	CO_3^{2-}	Na^+	PO_4^{3-}	log*K*
$(\equiv FeO)_2CO(b)$	BC	0	2	0	0.66	−0.66	0	2	1	0	0	21.73 ± 0.09[d]
$(\equiv FeO)_2CO\cdots Na(b)$	BCNa	0	2	0	0.65	0.35	0	2	1	1	0	22.38 ± 0.09[d]
$\equiv FeOCO_2(a)$	MC	1	0	0	0.34	−1.34	0	1	1	0	0	11.60 ± 0.01[d]
$\equiv FeOCO_2(b)$	MC	0	1	0	0.34	−1.34	0	1	1	0	0	11.60 ± 0.01[d]
$(\equiv FeO)_2PO_2(b)$	BP	0	2	0	0.46	−1.46	0	2	0	0	1	28.31 ± 0.04[e]
$(\equiv FeO)_2POOH(b)$	BPH	0	2	0	0.65	−0.65	0	3	0	0	1	33.52 ± 0.13[e]
$\equiv FeOPO_2OH(a)$	MPH	1	0	0	0.28	−1.28	0	2	0	0	1	26.36 ± 0.20[e]
$\equiv FeOPO_2OH(b)$	MPH	0	1	0	0.28	−1.28	0	2	0	0	1	26.36 ± 0.20[e]
$\equiv FeOPO(OH)_2(a)$	MPH2	1	0	0	0.33	−0.33	0	3	0	0	1	29.84 ± 0.23[e]
$\equiv FeOPO(OH)_2(b)$	MPH2	0	1	0	0.33	−0.33	0	3	0	0	1	29.84 ± 0.23[e]
		ρAN_{s1}[f]	ρAN_{s2}[f]	ρAN_{s3}[f]	Σ_1[f]	Σ_2[f]	Σ_3[f]	$H_{,tot}$	$CO_{3,tot}$	$Na_{,tot}$	$PO_{4,tot}$	

[a]The log*K* values for the CO_3 surfaces species were found by fitting the experimental results of the binary adsorption systems CO_3−PO_4 (n = 146). The surface site densities are from Hiemstra and Zhao[37] with ≡FeOH(a) = 3 nm^{-2}, ≡FeOH(b) = 2.8 nm^{-2}, and ≡Fe_3O = 1.4 nm^{-2}. The capacitance values for the extended Stern layer are C_1 = 1.15 F m^{-2} and C_2 = 0.9 F m^{-2}. [b]BC = Bidentate CO_3 inner-sphere; BCNa = Bidentate CO_3 inner-sphere with Na; MC = Monodentate CO_3 inner-sphere, BP = Bidentate PO_4 inner-sphere; BPH = Bidentate PO_4 inner-sphere protonated; MPH = Monodentate PO_4 inner-sphere protonated; MPH_2 = Monodentate PO_4 inner-sphere doubly protonated. [c]≡FeOH(a)$^{-0.5}$ forms only monodentate complexes with PO_4 and CO_3, whereas ≡FeOH(b)$^{-0.5}$ can form mono- and bidentate complexes, according to the ion adsorption model for Fh from Hiemstra and Zhao.[37] [d]log*K* (mean ± SD) are the average of the values obtained using four different fitting scales (see SI). [e]Taken from Hiemstra and Zhao.[37] [f]Sums of these columns are equal to the change of charge as defined Hiemstra and van Riemsdijk.[32]

Table 2. Charge Distribution Values (n_0, n_1) of Relevant CO_3^{2-} Surface Complexes Derived from the MO/DFT Optimized Geometries, Applying the Brown Bond Valence Concept[a]

Surface species	ID[b]	n_0[c]	n_1[c]	Δz_0	Δz_1	Δz_2
$(\equiv FeO)_2CO(b)$	BC	−1.40 ± 0.01	−0.60 ± 0.01	0.66	−0.66	0
$(\equiv FeO)_2CO\cdots Na(b)$	BCNa	−1.42 ± 0.02	−0.58 ± 0.02	0.65	0.35	0
$\equiv FeOCO_2(a)$	MC	−0.70 ± 0.01	−1.30 ± 0.01	0.34	−1.34	0
$\equiv FeOCO_2(b)$	MC	−0.70 ± 0.01	−1.30 ± 0.01	0.34	−1.34	0

[a]The CD coefficients (Δz_0, Δz_1) include the change of charge due to the reaction with protons (n_{H0}, n_{H1}) and a correction for the interfacial water dipole orientation. [b]BC = Bidentate CO_3 inner-sphere; BCNa = Bidentate CO_3 inner-sphere with Na; MC = Monodentate CO_3 inner-sphere. [c]Mean values (±SD) obtained from six different QC models (BP86, B3LYP, EDF1, EDF2, BLYP, ωP97X-D).

MO/DFT, i.e. Δz_0 = 0.34, Δz_1 = −1.34 v.u., which will be discussed in section 3.3.3.

The log*K* value for the above set of reactions is presented in Table 1 and corresponds to the average values found by evaluating the data at four different scales (i.e., % PO_4 adsorbed, PO_4 solution concentration, log PO_4 solution concentration, and μmol PO_4 adsorbed m^{-2}). In Table S-4 of the Supporting Information, the log*K* values fitted for each evaluation scale are given. The use of the parameter set presented in Table 1 and Table S-4 resulted in a good description of the entire data set (R^2 > 0.94, for all different scales).

Presently, we cannot entirely rule out for CO_3 the formation of an outer-sphere complex at the surfaces of Fh. In our modeling, considering the formation of outer-sphere complexes instead of the monodentate inner-sphere yields a similar quality of fitting (Appendix 4 in the SI) and describes the adsorption of CO_3 to Fh in monocomponent systems well. Spectroscopic information does suggest the formation of CO_3 outer-sphere complexes at the interfaces of Fe-(hydr)oxides. However, these complexes were particularly found at low pH and a low to very low ionic strength.[56] For other oxyanions (SeO_4^{2-}, CrO_4^{2-}, SO_4^{2-}), recent spectroscopy suggests a combination of inner- and outer-sphere complexes as mechanism to explain the adsorption to Fe-(hydr)-oxides.[47,60,61] However, all that presently matters is that according to the CD model any additional complex (either outer-sphere or inner-sphere complex) is contributing little in our systems. Binuclear bidentate complex formation of CO_3 is found to be dominant, as shown later in detail.

It is important to note that the introduction of a HCO_3^- surface complex did not improve the description of our data, yet HCO_3^- dominates the solution speciation of CO_3 over most of our experimental pH range. This agrees with the observation that surface complexes with CO_3^{2-} complexes dominate the surface speciation under atmospheric moisture conditions, whereas HCO_3^- complexes are only preferentially formed upon dehydration.[17,62,63] In addition, our optimization of the geometry of a monodentate HCO_3^- complex with MO/DFT shows that the proton of the adsorbed HCO_3 spontaneously shifts toward an adjacent ≡$FeOH^{-1/2}$ group if present in an O−H···O bond. This spontaneous shift leads formally to the formation of a ≡$FeOH_2^{+1/2}$ group and deprotonation of monodentate inner-sphere complex.

3.3.3. Charge Distribution Coefficients. In the CD model, the ionic charge of an inner-sphere complex is distributed over two different electrostatic planes at the interface. This interfacial charge distribution is accounted for by means of the CD coefficients (Δz_0, Δz_1). In the original approach,[32] the CD coefficients were estimated by assuming symmetrical distribution of the charge of the central ion over its ligands (Pauling bond valence). However, differences in the bonds lengths between the central ion and the coordinating ligands will lead to an asymmetrical charge distribution. Bond length differences can be interpreted with the semiempirical Brown

DOI: 10.1021/acsearthspacechem.8b00160
ACS Earth Space Chem. XXXX, XXX, XXX−XXX

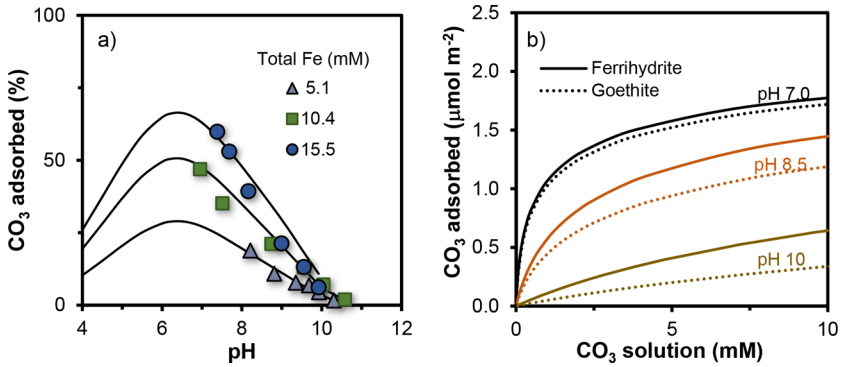

Figure 4. (a) Adsorption edges of CO_3 in single-ion systems with ferrihydrite at a constant ionic strength (I = 0.1 M $NaNO_3$). The black lines are CD model predictions using the parameter set of Table 1, that has been derived based on only interpreting competitive PO_4 adsorption data in carbonate systems. The adsorption edges are for systems with $CO_{3[T]}$ = 1 mM and three $Fe_{[T]}$ (5.1, 10.4, and 15.5 mM). The specific surface area of ferrihydrite was A = 625 m^2 g^{-1} at a corresponding molar mass of M_{nano} = 95.14 g mol^{-1} Fe. (b) Modeled adsorption isotherms of CO_3 to ferrihydrite (full lines) and goethite (dotted lines) at a constant ionic strength (I = 0.10 M) and three pH values: 7.0, 8.5, and 10.0. Model parameters for ferrihydrite are from Table 1, whereas for goethite they are taken from Rahnemaie et al.[29]

valence concept,[34,35] which relates bond length (R) to a bond valence (s).

In our approach, we have used MO/DFT calculations to optimize the geometry of a series of different CO_3−Fe complexes and derive subsequently the values of the CD coefficients. This approach has the advantage of restricting the number of adjustable parameters per surface species to one (i.e., log$K$). The optimized geometries of the relevant CO_3 surface complexes used in the final modeling are presented in the graph of the table of contents (TOC).

In Table 2, the ionic charge distribution values (n_0, n_1) are presented for the different CO_3 surface species considered in our modeling (section 3.3.2). Detailed information about the bond length distances and the application of the Brown bond concept is given in Appendix 9 of the SI. The final CD coefficients (Δz_0, Δz_1) include the change of charge that results from the protons involved (n_{H0}, n_{H1}) in the formation reactions (eqs 6−8). In addition, there is a correction term ($\pm\varphi_m$ Λ_0) for the interfacial water dipole orientation. The factor φ_m is a constant (0.17 ± 0.02),[42] and Λ_0 is the change of charge relatively to that of the reference state from which the reaction is defined. Therefore, $\Lambda_0 = n_0 + n_{H0} + \Sigma\, n_{ref} \times z_{ref}$ in which n_{ref} and z_{ref} are the number and the charge of the reference surface groups involved, respectively.[39]

As follows from the n_0 and n_1 values presented in Table 2, there is some asymmetry in the distribution of the central C^{4+} charge over the different -O ligands of the CO_3 surface complexes. Slightly more negative charge is attributed to the Fe−O−C bonds in comparison to the symmetrical charge distribution according to the Pauling bond valence concept. The interaction of the bidentate carbonate complex with a Na^+ ion does not affect significantly the n_0 and n_1 values of the O-ligands in this ternary complex, which implies that no significant transfer of charge occurs from the Na^+ to the O-ligands of the bidentate complex. Free fitting of the CD coefficients of the BCNa complex suggests a full attribution of the Na^+ charge to the 1-plane of the Stern layer. The Δz_1 value of the BCNa complex in Table 2 includes the charge of Na^+.

The results presented in Table 2 are for complexes optimized using an uncharged $(H_2O)_2Fe_2(OH)_6(OH_2)_2$ template (A) that has also been used previously to derive the CD coefficients for the PO_4 surface species.[37,42] It has been shown that the charge of the template may influence the calculated CD coefficients;[29] that is, the charge distribution may depend on the protonation/deprotonation of the overall moiety.[5] Calculations performed with a positive charged template, $(H_2O)_2Fe_2(OH)_4(OH_2)_4$ (B) resulted in more transfer of negative charge (−0.09 v.u.) to the common O-ligands for the binuclear bidentate CO_3 complexes in comparison with template A. Nevertheless, this variation was still lower in comparison with the uncertainty of the CD coefficients (±0.25 v.u.) found at free fitting of the CD value using our experimental data. For the CO_3−PO_4 competition experiments, the same quality of the fitting was obtained using either template A or B as model. However, use of template A leads to a better prediction of the adsorption of CO_3 in monocomponent systems.

3.4. Model Applications. *3.4.1. Carbonate Adsorption in Single-Ion Systems.* The suitability of the above-derived CD model parameters for describing the adsorption of CO_3 in single-ion systems with Fh will be evaluated here. Batch adsorption experiments were performed using three $Fe_{[T]}$ levels (5.1, 10.4, and 15.5 mM) at a fixed initial $CO_{3[T]}$ of 1 mM and a constant ionic strength of 0.10 M $NaNO_3$. The pH of the systems varied from 6.9 to 10.5. As shown in Figure 4a, the adsorption of CO_3 to Fh continuously decreases as the solution pH increases from 7 to 10 (symbols). The solid lines are the corresponding CD model predictions for the adsorption of CO_3 in these systems, using the parameter values of Table 1. Interestingly, these parameters have been derived without any direct measurement of the CO_3 adsorption. The excellent prediction obtained for the single-ion systems shows that the CD model can be well parametrized for CO_3 by only measuring the competitive effect of this anion on the adsorption of PO_4 to Fh. In addition, it is noted that the total concentration of CO_3 is 4 to 500 times lower in the single-ion experiments than applied in the competition experiments. The good agreement between the experimental adsorption edges and the model predictions evidences the reliability of the CD model to describe the adsorption of CO_3 over a broad range of conditions. This is highly relevant from an environmental point of view as CO_3 is omnipresent in soils, sediments, rivers, groundwater, and marine systems at highly variable conditions. It will contribute to an improved modeling of the geochemical cycle of a range of compounds relevant from the environmental perspective.[64−66]

DOI: 10.1021/acsearthspacechem.8b00160
ACS Earth Space Chem. XXXX, XXX, XXX−XXX

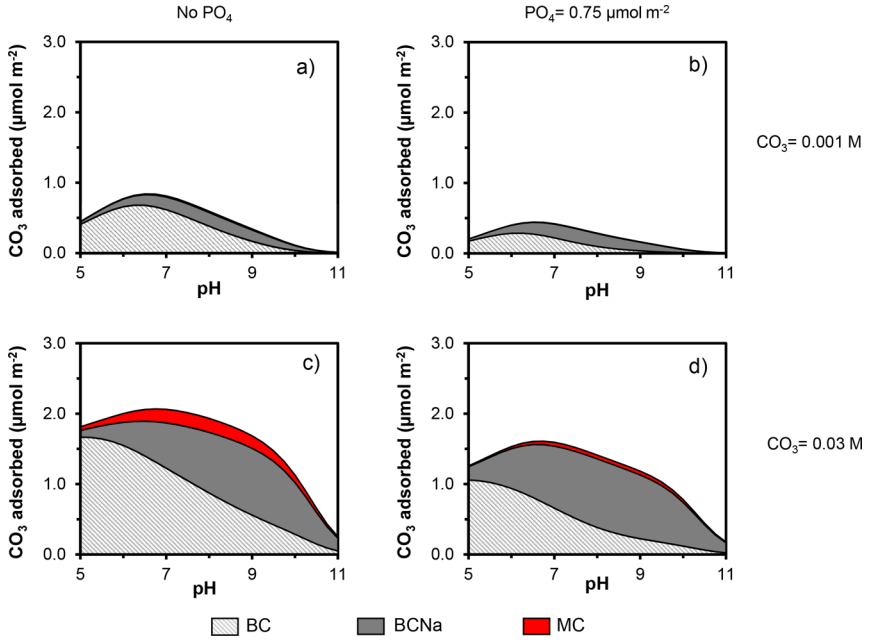

Figure 5. Surface speciation of CO_3 on ferrihydrite as a function of pH for single CO_3 systems (left panels) and binary CO_3−PO_4 systems (right panels). The CD model calculations were performed with the CO_3 and PO_4 parameter set presented Table 1. The upper panels (a and b) are for systems with a $CO_{3[T]}$ = 0.001 M, whereas the lower panels (c and d) are for systems with $CO_{3(T)}$ = 0.03 M. The ferrihydrite concentration was 0.5 g L^{-1} with an assumed SSA of 670 m^2 g^{-1}. The ionic strength in all the systems was adjusted at 0.05 M by adding $NaNO_3$.

According to our model simulations (Figure 4a), the adsorption maximum of CO_3 to Fh occurs around pH 6.5−7.0. This maximum is nearly independent from the solid-to-solution ratio of the system. Above pH ∼6.5, the CO_3 adsorption decreases at increase of pH, while the opposite occurs below pH ∼6.5. This behavior has also been found for goethite by Villalobos and Leckie[16] and can be predicted very well with the CD model.[29] A similar pH-dependency has also been found by Zachara et al.[24] for single-ion systems with Fh. Even though measured for very low CO_3 concentrations (i.e., μM levels), the pH-dependency of this data set can also be predicted well with the present CD model (Table 1), as shown in Figure S-6 in the Supporting Information.

The characteristic pH-dependency of the CO_3 adsorption with a maximum in the adsorption edge (Figure 4a) is due to a change in solution speciation. The pH-dependency of adsorption is a trade-off between proton binding to surface and solution species. According to the thermodynamic consistency principle,[39,67,68] the change (∂) of the logarithm of the solution concentration with pH is

$$\left(\frac{\partial \log C_{CO3(T)}}{\partial pH}\right)_{\Gamma_{CO3}} = (\chi_H - n_H)_{pH} \quad (9)$$

in which χ_H is the molar ratio of the proton excess adsorption upon adsorption of CO_3, known as proton coadsorption ratio, and n_H is the mean number of protons bound to dissolved CO_3 species, both defined relatively to a chosen reference species. Calculations show that the proton coadsorption is about χ_H∼ 1.5 at neutral pH. Using CO_3^{2-}(aq) as reference, n_H = +2 when H_2CO_3(aq) dominates the system at pH < logK_{H2} = 6.35, and $\chi_H - n_H$ < 0, while $\chi_H - n_H$ > 0 for n_H = +1 in a solution dominated by HCO_3^-(aq) (pH > 6.35). The change of n_H leads to the remarkable switch in pH-dependency shown in Figure 4a. At pH ∼ logK_{H2}, n_H = 1.5 and $\chi_H - n_H$ ∼ 0. This implies that at this condition, there will be no pH-dependency of the CO_3 adsorption. This coincides with the top of the curves in Figure 4a. The above thermodynamic consistency principle can also be applied to the adsorption of other ions, including the adsorption of Si to Fh, as discussed recently in detail.[5]

In Figure 4b, the modeled adsorption isotherms of CO_3 to Fh (full lines) are presented for systems at pH 7.0, 8.5, and 10.0. For comparison, the corresponding adsorption isotherms to goethite (α-FeOOH) have also been modeled (dotted lines), using the CD model parameters from Rahnemaie et al.[29] At pH 7.0, the adsorption of CO_3 to both Fe-(hydr)oxide minerals is similar over the entire range of solution concentrations. As the pH increases, more CO_3 is adsorbed to Fh than to goethite, under similar solution conditions. This difference is more significant at increased CO_3 loadings, and it can be related to differences in the surface speciation of CO_3 of both minerals. Particularly important is the enhanced formation of the BCNa complex in the Fh systems. Formulating the formation of the BCNa complex according to

$$\equiv(FeO)_2^{-1+\Delta z_0}CO^{\Delta z_1} + Na^+(aq) \Leftrightarrow \equiv(FeO)_2^{-1+\Delta z_0}CO\cdots Na^{+1+\Delta z_1} \quad (10)$$

the corresponding equilibrium constant of the reaction is log K + 0.65 for Fh and log K + 0.02 for goethite. The difference shows that for a given solution condition, the formation of the BCNa is more favored at the surfaces of Fh. The pH and concentration dependence of the CO_3 surface speciation in Fh is presented in Figure 5 and Figure S-5 (see SI), respectively.

3.4.2. Carbonate Surface Speciation. In this section, we evaluate the effect of pH, $CO_{3(T)}$, and the presence of PO_4 on the surface speciation of adsorbed CO_3 (Figure 5). It is observed that the distribution of the adsorbed CO_3 over the different surface species is strongly affected by the pH of the solution. The BC complex is the dominant CO_3 surface species in the low pH range (Figure 5a−d). As the pH increases, the

DOI: 10.1021/acsearthspacechem.8b00160
ACS Earth Space Chem. XXXX, XXX, XXX−XXX

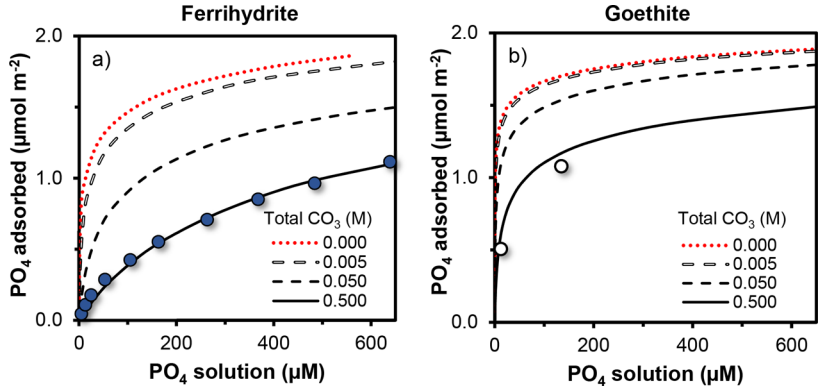

Figure 6. Panel a: Adsorption isotherm of PO_4 to ferrihydrite in 0.5 M $NaHCO_3$ at pH 8.70 ± 0.01. The specific surface area of the ferrihydrite was A = 735 m^2 g^{-1} with a respective molar mass of M_{nano} = 97.98 g mol^{-1} Fe. The total reactive area was 375 m^2 L^{-1}. The symbols are experimental data and the (full) line is the model prediction. For comparison, the calculated PO_4 adsorption isotherms for systems with 0 (red dotted line), 0.005 (open-dashed line), and 0.05 M (dashed line) $CO_{3[T]}$ have also been included in the graph. The ionic strength was fixed at 0.5 M by adding $NaNO_3$ when required. CD model calculations were performed with the parameters presented in Table 1. Panel b: Modeled adsorption isotherms of PO_4 to goethite in the absence (red dotted line) and presence (black lines) of CO_3 for the same solution as used in panel a. Modeling parameters and PO_4 adsorption data points were taken from Rahnemaie et al.[29]

relative contribution of the BCNa complex to the total CO_3 adsorption gradually increases. The relative importance of the BCNa complex further increases at a high loading of CO_3 and/or PO_4 (Figure 5c and d), which can be understood from the increase of the negative value of the electrostatic potential in the inner Stern (1-) plane. This leads for the Na^+ ions to a stronger attraction and formation of the ternary surface species.

Figure 5 also depicts that the formation of the MC complex is almost negligible at a low $CO_{3[T]}$ level (Figures 5a and b vs c and d). This fits with our modeling experience (section 3.3.2) that the incorporation of this MC species was only necessary to describe the results of the CO_3–PO_4 competition experiments at the high $CO_{3[T]}$ levels. In addition, comparison of the single and binary ion systems (Figures 5c vs d) shows that at the chosen $CO_{3[T]}$ level, the formation of the MC complex is reduced when PO_4 is present. This effect also follows from electrostatic considerations. As mentioned before, the specific adsorption of PO_4 induces uncompensated negative charge that increases the negative electrostatic potential of the inner Stern or 1-plane (see Figure S-7 in the Supporting Information). Since MC complex introduces more negative charge in the 1-plane (Δz_1 = −1.34 v.u.) than BC complexes (Δz_1 = −0.66 v.u.), the formation of the former surface complex is most suppressed in the presence of PO_4.

3.4.3. PO_4 Extraction with Carbonate Solution. The competitive interaction CO_3–PO_4 has been traditionally used in soil chemical analysis to evaluate the soil PO_4 availability in natural and agricultural systems.[69,70] More recently, this interaction has been applied to derive the effective reactive surface area (RSA) of soils.[31] In the present study, we have measured the PO_4 adsorption isotherm for Fh in 0.5 M $NaHCO_3$ (pH = 8.70 ± 0.01) over a range of equilibrium PO_4 concentrations (~5–650 μM) that represents the conditions typically found when natural and fertilized field samples are extracted with 0.5 M $NaHCO_3$.[70] The lines in Figure 6a are predictions with the CD model, showing an accurate prediction of the PO_4 adsorption density (μmol m^{-2}) for the systems in competition with CO_3, using the set of adsorption parameters presented in Table 1.

As an example of the competitive effect of added $NaHCO_3$ at a pH condition relevant in soil extractions, additional PO_4 adsorption isotherms have been calculated for systems with an increasing $CO_{3[T]}$ (dashed lines), as well as for systems with no CO_3 addition (red dotted line). CO_3 is a good competitor at high concentrations, removing a significant amount of adsorbed PO_4 from the surfaces of Fh. It diminishes the high affinity character (shape) of the PO_4 adsorption isotherm (Figure 6a).

Figure 6b shows the adsorption isotherms of PO_4 for goethite (α-FeOOH) calculated with the CD model parameters derived by Rahnemaie et al.[29] This latter material has been used to derive the RSA soil samples, while results suggest that the natural oxide fraction is dominated by nanoparticles (e.g., Fh).[31] In the absence of CO_3, the adsorption of PO_4 is similar in both Fe-(hydr)oxide materials. However, CO_3 removes less PO_4 from goethite than from Fh at the same solution conditions. The PO_4 adsorption isotherm in goethite remains steeper. The results in Figure 6 agree with the model simulations presented previously in Figure 4b, which showed that at high pH, CO_3 has a higher adsorption affinity for Fh than for goethite. This results in a stronger competition with PO_4 in the systems with Fh.

With the collected information on Figure 6, one may assess the RSA (m^2 g^{-1} soil) based on the change (Δ) of the PO_4 amount in solution and the change in surface loading $\Delta\Gamma_{PO_4}$ (mol m^{-2}), according to

$$\mathrm{RSA} = \frac{\Delta(c_{PO_4} \times \mathrm{SSR})}{\Delta\Gamma_{PO_4}} \tag{11}$$

in which c_{PO_4} is the experimental PO_4 concentration (mol L^{-1}) and SSR is the solution-to-soil ratio (in L kg^{-1}). The measured change in concentration Δc_{PO4} (mol L^{-1}) is translated into a corresponding change in PO_4 surface loading $\Delta\Gamma_{PO4}$ (μmol m^{-2}) calculated with the CD model.

As follows from Figure 6, the relation between Δc_{PO4} and $\Delta\Gamma_{PO4}$ value is clearly determined by the slope of the adsorption isotherm and consequently depends on the type of Fe-(hydr)oxide used as reference material. A steeper adsorption isotherm will lead to more buffering of the PO_4 concentration, i.e. smaller Δc_{PO4} at the same $\Delta\Gamma_{PO4}$, leading to a lower value for the calculated RSA. In 0.5 M $NaHCO_3$, goethite has a PO_4 adsorption isotherm that is relatively flat at

DOI: 10.1021/acsearthspacechem.8b00160
ACS Earth Space Chem. XXXX, XXX, XXX–XXX

a high PO_4 concentration compared to Fh. This implies that its use as reference oxide to calculate the reactive surface area of soils will lead to higher values than with the use of Fh as reference oxide. This illustrates that precise information about the adsorption isotherm of the natural oxide fraction is essential for a correct assessment of the effective RSA of soil samples. In a forthcoming contribution, we will evaluate the use of Fh as nanoparticulate proxy for the natural metal oxide fraction of soils by applying the information collected in the present study.

4. CONCLUSIONS

In the present study, we aim to quantify the interaction of CO_3 with Fh by measuring its competitive effect on the adsorption of PO_4 in closed systems. Our analysis starts by evaluating the effect of high CO_3 concentrations on the solubility of Fh, since Fe(III)-CO_3 complexes may form while our freshly prepared Fh is relatively soluble. Three aqueous species FeOH-CO_3^0(aq), $Fe(CO_3)_3^{3-}$(aq), and $Fe(CO_3)_2(OH)_2^{3-}$(aq) are found to be relevant according to modeling literature[38] and our own data. The latter species is most important in our closed systems, while both others are more relevant in open systems. At the chosen conditions in the adsorption experiments, only a very small fraction of Fh (<0.4%) was dissolved, enabling straightforward interpretation of the collected CO_3 adsorption data.

CO_3 competes with PO_4 for the adsorption sites of the Fh surface. However, PO_4 has a significantly larger affinity than CO_3 for these binding sites, meaning that high CO_3/PO_4 concentration ratios are needed to remove PO_4 efficiently from the surface of Fh. The competitive interaction CO_3−PO_4 in Fh systems was successfully described with the CD model using only the experimental PO_4 adsorption data for parametrization. The CD coefficients of the CO_3 surfaces complexes were derived independently from the MO/DFT optimized geometries. Our study provides insights into the surface speciation of CO_3 that are consistent with the state-of-the-art knowledge of the mineral and surface structure of Fh. CO_3 is predominantly bound as an inner-sphere bidentate (double-corner) complex. At high CO_3 and/or PO_4 loading and a high Na^+ concentration, this $\equiv(FeO)_2CO$ complex interacts with Na^+ forming a ternary $\equiv(FeO)_2CO\cdots Na^+$ complex in which Na^+ most likely forms an ion pair with the adsorbed CO_3. At high CO_3 loading, an additionally surface complex is formed that may be an inner-sphere monodentate complex ($\equiv FeOCO_2$).

We have shown that the CD model, only parametrized with the PO_4 adsorption data from the CO_3−PO_4 competition experiments, can predict the experimental adsorption of CO_3 in monocomponent systems with $CO_{3[T]}$ levels that are relevant in the natural environment (soil, river, groundwater, and seawater). The adsorption of CO_3 in the monocomponent systems reaches a maximum at pH ∼6.5 in full agreement with literature results and is thermodynamically consistent with the surface speciation derived. Our CD modeling demonstrates that the CO_3 surface speciation is mainly governed by effects of charge, particularly acting on the potential of the inner Stern layer. Change in environmental conditions such as pH, ionic strength, and concentration of competitive anions will change the relative distribution over the different CO_3 surface species.

Finally, it is shown that our CD model can predict very well the measured adsorption isotherm of PO_4 in Fh systems with 0.5 M $NaHCO_3$ at high pH. In comparison with goethite, CO_3 has a significantly higher adsorption affinity to Fh, which leads to a marked decrease in the high affinity character of the adsorption isotherm of PO_4 in 0.5 M $NaHCO_3$. The higher adsorption of CO_3 to Fh is particularly evident at high pH values, and it is related to the enhanced interaction of Na^+ with the BC complex forming BCNa. The parametrized CO_3−PO_4 interaction can be used to interpret the equilibration data of soil extractions in 0.5 M $NaHCO_3$ solution to reveal RSA, using Fh as reference material for the natural oxide fraction. A consistent determination of the RSA may improve the prediction of the adsorption behavior of nutrients and pollutants in environmental samples with surface complexation modeling.

■ ASSOCIATED CONTENT

Supporting Information

The Supporting Information is available free of charge on the ACS Publications website at DOI: 10.1021/acsearthspacechem.8b00160.

Experimental conditions of the batch experiments (1), Additional phosphate adsorption experiments (2), Thermodynamic databases used in the CD modeling (3), Evaluation of carbonate adsorption parameters at different scales (4), Aqueous complex formation of Fe(III)-carbonates (5), Normalized competitive adsorption isotherms (6), Adsorption isotherms: carbonate surface speciation (7), Adsorption data of carbonate from literature (8), Bond length and Brown bond valence concept (9), Effect of phosphate adsorption on the surface charge of ferrihydrite (10) (PDF)

■ AUTHOR INFORMATION

Corresponding Author

*E-mail address: juan.mendezfernandez@wur.nl.

ORCID

Juan C. Mendez: 0000-0002-1658-400X

Notes

The authors declare no competing financial interest.

■ ACKNOWLEDGMENTS

We highly appreciate the work of Jelle Jansen in collecting part of the CO_3−PO_4 competition data. We are also grateful for the accurate and attentive work regarding the sample analysis by Peter Nobels and Johan Uijtenbroek, from the Chemistry and Biology Soil Laboratory (CBLB). The grant provided by the University of Costa Rica (UCR) to the first author is gratefully acknowledged.

■ REFERENCES

(1) Hochella, M. F.; Lower, S. K.; Maurice, P. A.; Penn, R. L.; Sahai, N.; Sparks, D. L.; Twining, B. S. Nanominerals, mineral nanoparticles, and earth systems. *Science (Washington, DC, U. S.)* **2008**, *319* (5870), 1631−1635.

(2) van der Zee, C.; Roberts, D. R.; Rancourt, D. G.; Slomp, C. P. Nanogoethite is the dominant reactive oxyhydroxide phase in lake and marine sediments. *Geology* **2003**, *31* (11), 993−996.

(3) Hiemstra, T.; Antelo, J.; van Rotterdam, A. M. D.; van Riemsdijk, W. H. Nanoparticles in natural systems II: The natural oxide fraction at interaction with natural organic matter and phosphate. *Geochim. Cosmochim. Acta* **2010**, *74* (1), 59−69.

(4) Wang, X.; Kubicki, J. D.; Boily, J. F.; Waychunas, G. A.; Hu, Y.; Feng, X.; Zhu, M. Binding geometries of silicate species on ferrihydrite surfaces. *ACS Earth Sp. Chem.* **2018**, *2* (2), 125−134.

DOI: 10.1021/acsearthspacechem.8b00160
ACS Earth Space Chem. XXXX, XXX, XXX−XXX

(5) Hiemstra, T. Ferrihydrite interaction with silicate and competing oxyanions: Geometry and hydrogen bonding of surface species. *Geochim. Cosmochim. Acta* **2018**, *238*, 453−476.
(6) Liu, J.; Zhu, R.; Liang, X.; Ma, L.; Lin, X.; Zhu, J.; He, H.; Parker, S. C.; Molinari, M. Synergistic adsorption of Cd(II) with sulfate/phosphate on ferrihydrite: An in situ ATR-FTIR/2D-COS study. *Chem. Geol.* **2018**, *477*, 12−21.
(7) Zhang, Y.; Wu, B.; Xu, H.; Liu, H.; Wang, M.; He, Y.; Pan, B. Nanomaterials-enabled water and wastewater treatment. *NanoImpact* **2016**, *3*−*4*, 22−39.
(8) Xu, P.; Zeng, G. M.; Huang, D. L.; Feng, C. L.; Hu, S.; Zhao, M. H.; Lai, C.; Wei, Z.; Huang, C.; Xie, G. X.; et al. Use of iron oxide nanomaterials in wastewater treatment: A review. *Sci. Total Environ.* **2012**, *424*, 1−10.
(9) Gora, S.; Liang, R.; Zhou, Y. N.; Andrews, S. Settleable engineered titanium dioxide nanomaterials for the removal of natural organic matter from drinking water. *Chem. Eng. J.* **2018**, *334*, 638−649.
(10) Michel, F. M.; Ehm, L.; Antao, S. M.; Lee, P. L.; Chupas, P. J.; Liu, G.; Strongin, D. R.; Schoonen, M. A. A.; Phillips, B. L.; Parise, J. B. The structure of ferrihydrite, a nanocrystalline material. *Science* **2007**, *316* (5832), 1726−1729.
(11) Hiemstra, T. Surface and mineral structure of ferrihydrite. *Geochim. Cosmochim. Acta* **2013**, *105*, 316−325.
(12) Jambor, J. L.; Dutrizac, J. E. Occurrence and constitution of natural and synthetic ferrihydrite, a widespread iron oxyhydroxide. *Chem. Rev.* **1998**, *98* (7), 2549−2586.
(13) Guo, H.; Barnard, A. S. Naturally occurring iron oxide nanoparticles: morphology, surface chemistry and environmental stability. *J. Mater. Chem. A* **2013**, *1* (1), 27−42.
(14) Hiemstra, T. Formation, stability, and solubility of metal oxide nanoparticles: Surface entropy, enthalpy, and free energy of ferrihydrite. *Geochim. Cosmochim. Acta* **2015**, *158*, 179−198.
(15) Stumm, W.; Morgan, J. J. *Aquatic chemistry: chemical equilibria and rates in natural waters*; John Wiley & Sons, 2012; Vol. *126*.
(16) Villalobos, M.; Leckie, J. O. Carbonate adsorption on goethite under closed and open CO2 conditions. *Geochim. Cosmochim. Acta* **2000**, *64* (22), 3787−3802.
(17) Hausner, D. B.; Bhandari, N.; Pierre-Louis, A. M.; Kubicki, J. D.; Strongin, D. R. Ferrihydrite reactivity toward carbon dioxide. *J. Colloid Interface Sci.* **2009**, *337* (2), 492−500.
(18) Taifan, W.; Boily, J.-F.; Baltrusaitis, J. Surface chemistry of carbon dioxide revisited. *Surf. Sci. Rep.* **2016**, *71* (4), 595−671.
(19) Ostergren, J. D.; Brown, G. E.; Parks, G. A.; Persson, P. Inorganic ligand effects on Pb(II) sorption to goethite (α- FeOOH) - II. Sulfate. *J. Colloid Interface Sci.* **2000**, *225* (2), 483−493.
(20) Wazne, M.; Korfiatis, G. P.; Meng, X. Carbonate effects on hexavalent uranium adsorption by iron oxyhydroxide. *Environ. Sci. Technol.* **2003**, *37* (16), 3619−3624.
(21) Hiemstra, T.; Van Riemsdijk, W. H.; Rossberg, A.; Ulrich, K.-U. A surface structural model for ferrihydrite II: Adsorption of uranyl and carbonate. *Geochim. Cosmochim. Acta* **2009**, *73* (15), 4437−4451.
(22) Appelo, C. A. J.; Van Der Weiden, M. J. J.; Tournassat, C.; Charlet, L. Surface complexation of ferrous iron and carbonate on ferrihydrite and the mobilization of arsenic. *Environ. Sci. Technol.* **2002**, *36* (14), 3096−3103.
(23) Stachowicz, M.; Hiemstra, T.; Van Riemsdijk, W. H. Arsenic-bicarbonate interaction on goethite particles. *Environ. Sci. Technol.* **2007**, *41* (16), 5620−5625.
(24) Zachara, J. M.; Girvin, D. C.; Schmidt, R. L.; Resch, C. T. Chromate adsorption on amorphous iron oxyhydroxide in the presence of major groundwater ions. *Environ. Sci. Technol.* **1987**, *21* (6), 589−594.
(25) van Geen, A.; Robertson, A. P.; Leckie, J. O. Complexation of carbonate species at the goethite surface: Implications for adsorption of metal ions in natural waters. *Geochim. Cosmochim. Acta* **1994**, *58* (9), 2073−2086.
(26) Brechbühl, Y.; Christl, I.; Elzinga, E. J.; Kretzschmar, R. Competitive sorption of carbonate and arsenic to hematite: Combined ATR-FTIR and batch experiments. *J. Colloid Interface Sci.* **2012**, *377* (1), 1−18.
(27) Biswas, A.; Gustafsson, J. P.; Neidhardt, H.; Halder, D.; Kundu, A. K.; Chatterjee, D.; Berner, Z.; Bhattacharya, P. Role of competing ions in the mobilization of arsenic in groundwater of Bengal Basin: Insight from surface complexation modeling. *Water Res.* **2014**, *55*, 30−39.
(28) Peter, A.; Lamert, H.; Beyer, M.; Hornbruch, G.; Heinrich, B.; Schulz, A.; Geistlinger, H.; Schreiber, B.; Dietrich, P.; Werban, U.; et al. Investigation of the geochemical impact of CO2 on shallow groundwater: design and implementation of a CO2 injection test in Northeast Germany. *Environ. Earth Sci.* **2012**, *67* (2), 335−349.
(29) Rahnemaie, R.; Hiemstra, T.; van Riemsdijk, W. H. Carbonate adsorption on goethite in competition with phosphate. *J. Colloid Interface Sci.* **2007**, *315* (2), 415−425.
(30) Flower, H.; Rains, M.; Lewis, D.; Zhang, J.-Z.; Price, R. Control of phosphorus concentration through adsorption and desorption in shallow groundwater of subtropical carbonate estuary. *Estuarine, Coastal Shelf Sci.* **2016**, *169*, 238−247.
(31) Hiemstra, T.; Antelo, J.; Rahnemaie, R.; van Riemsdijk, W. H. Nanoparticles in natural systems I: The effective reactive surface area of the natural oxide fraction in field samples. *Geochim. Cosmochim. Acta* **2010**, *74* (1), 41−58.
(32) Hiemstra, T.; Van Riemsdijk, W. H. A surface structural approach to ion adsorption: The charge distribution (CD) model. *J. Colloid Interface Sci.* **1996**, *179* (2), 488−508.
(33) Michel, F. M.; Barron, V.; Torrent, J.; Morales, M. P.; Serna, C. J.; Boily, J.-F.; Liu, Q.; Ambrosini, A.; Cismasu, A. C.; Brown, G. E. Ordered ferrimagnetic form of ferrihydrite reveals links among structure, composition, and magnetism. *Proc. Natl. Acad. Sci. U. S. A.* **2010**, *107* (7), 2787−2792.
(34) Brown, I. D.; Altermatt, D. Bond-valence parameters obtained from a systematic analysis of the inorganic crystal structure database. *Acta Crystallogr., Sect. B: Struct. Sci.* **1985**, *41* (4), 244−247.
(35) Brown, I. D. Recent developments in the methods and applications of the bond valence model. *Chem. Rev.* **2009**, *109* (12), 6858−6919.
(36) Hiemstra, T.; Van Riemsdijk, W. H. A surface structural model for ferrihydrite I: Sites related to primary charge, molar mass, and mass density. *Geochim. Cosmochim. Acta* **2009**, *73* (15), 4423−4436.
(37) Hiemstra, T.; Zhao, W. Reactivity of ferrihydrite and ferritin in relation to surface structure, size, and nanoparticle formation studied for phosphate and arsenate. *Environ. Sci.: Nano* **2016**, *3*, 1265−1279.
(38) Grivé, M.; Duro, L.; Bruno, J. Fe(III) mobilisation by carbonate in low temperature environments: Study of the solubility of ferrihydrite in carbonate media and the formation of Fe(III) carbonate complexes. *Appl. Geochem.* **2014**, *49*, 57−67.
(39) Hiemstra, T.; Van Riemsdijk, W. H. On the relationship between charge distribution, surface hydration, and the structure of the interface of metal hydroxides. *J. Colloid Interface Sci.* **2006**, *301* (1), 1−18.
(40) Keizer, M. G.; van Riemsdijk, W. H.ECOSAT, Equilibrium Calculation of Speciation and Transport. Technical Report. Department of Soil Quality. Wageningen Univeristy; 1998.
(41) Kinniburgh, D. G. *Fit, Technical Report WD/93/23*; Keyworth, Great Britain, 1993.
(42) Rahnemaie, R.; Hiemstra, T.; Van Riemsdijk, W. H. Geometry, charge distribution, and surface speciation of phosphate on goethite. *Langmuir* **2007**, *23* (7), 3680−3689.
(43) Bruno, J.; Stumm, W.; Wersin, P.; Brandberg, F. On the influence of carbonate in mineral dissolution: I. The thermodynamics and kinetics of hematite dissolution in bicarbonate solutions at T = 25°C. *Geochim. Cosmochim. Acta* **1992**, *56* (3), 1139−1147.
(44) Hummel, W.; Bruno, J.; Stumm, W.; Wersin, P.; Brandberg, F. Comment on "On the influence of carbonate in mineral dissolution: 1. The thermodynamics and kinetics of hematite dissolution in bicarbonate solutions at T = 25°C" by. *Geochim. Cosmochim. Acta* **2000**, *64* (12), 2167−2171.

DOI: 10.1021/acsearthspacechem.8b00160
ACS Earth Space Chem. XXXX, XXX, XXX−XXX

(45) Antelo, J.; Fiol, S.; Pérez, C.; Mariño, S.; Arce, F.; Gondar, D.; López, R. Analysis of phosphate adsorption onto ferrihydrite using the CD-MUSIC model. *J. Colloid Interface Sci.* **2010**, *347* (1), 112−119.
(46) Stachowicz, M.; Hiemstra, T.; van Riemsdijk, W. H. Multi-competitive interaction of As(III) and As(V) oxyanions with Ca2+, Mg2+, PO3−4, and CO2−3 ions on goethite. *J. Colloid Interface Sci.* **2008**, *320* (2), 400−414.
(47) Gu, C.; Wang, Z.; Kubicki, J. D.; Wang, X.; Zhu, M. X-ray absorption spectroscopic quantification and speciation modeling of sulfate adsorption on ferrihydrite surfaces. *Environ. Sci. Technol.* **2016**, *50* (15), 8067−8076.
(48) Arai, Y.; Sparks, D. L. ATR−FTIR spectroscopic investigation on phosphate adsorption mechanisms at the ferrihydrite−water interface. *J. Colloid Interface Sci.* **2001**, *241* (2), 317−326.
(49) Mallet, M.; Barthélémy, K.; Ruby, C.; Renard, A.; Naille, S. Investigation of phosphate adsorption onto ferrihydrite by X-ray Photoelectron Spectroscopy. *J. Colloid Interface Sci.* **2013**, *407*, 95−101.
(50) Goldberg, S.; Johnston, C. T. Mechanisms of arsenic adsorption on amorphous oxides evaluated using macroscopic measurements, vibrational spectroscopy, and surface complexation modeling. *J. Colloid Interface Sci.* **2001**, *234* (1), 204−216.
(51) Villalobos, M.; Leckie, J. O. Surface complexation modeling and FTIR study of carbonate adsorption to goethite. *J. Colloid Interface Sci.* **2001**, *235* (1), 15−32.
(52) Wijnja, H.; Schulthess, C. P. Carbonate adsorption mechanism on goethite studied with ATR − FTIR, DRIFT, and proton coadsorption measurements. *Soil Sci. Soc. Am. J.* **2001**, *65* (2), 324−330.
(53) Su, C.; Suarez, D. L. In situ infrared speciation of absorbed carbonate on aluminum and iron oxides. *Clays Clay Miner.* **1997**, *45*, 814−825.
(54) Goldsmith, J. A.; Ross, S. D. Factors affecting the infra-red spectra of planar anions with D3h symmetry—IV The vibrational spectra of some complex carbonates in the region 4000−400 cm−1. *Spectrochim. Acta Part A Mol. Spectrosc.* **1968**, *24* (8), 993−998.
(55) Hiemstra, T.; Rahnemaie, R.; Van Riemsdijk, W. H. Surface complexation of carbonate on goethite: IR spectroscopy, structure and charge distribution. *J. Colloid Interface Sci.* **2004**, *278* (2), 282−290.
(56) Bargar, J. R.; Kubicki, J. D.; Reitmeyer, R.; Davis, J. A. ATR-FTIR spectroscopic characterization of coexisting carbonate surface complexes on hematite. *Geochim. Cosmochim. Acta* **2005**, *69* (6), 1527−1542.
(57) Kubicki, J. D.; Kwon, K. D.; Paul, K. W.; Sparks, D. L. Surface complex structures modelled with quantum chemical calculations: Carbonate, phosphate, sulphate, arsenate and arsenite. *Eur. J. Soil Sci.* **2007**, *58* (4), 932−944.
(58) Capewell, S. G.; Buchner, R.; Hefter, G.; May, P. M. Dielectric relaxation of aqueous Na2CO3 solutions. *Phys. Chem. Chem. Phys.* **1999**, *1* (8), 1933−1937.
(59) Rudolph, W. W.; Irmer, G.; Königsberger, E. Speciation studies in aqueous HCO_3^- − CO_3^{2-} solutions. A combined Raman spectroscopic and thermodynamic study. *Dalt. Trans.* **2008**, *0* (7), 900−908.
(60) Johnston, C. P.; Chrysochoou, M. Mechanisms of chromate, selenate, and sulfate adsorption on Al-substituted ferrihydrite: Implications for ferrihydrite surface structure and reactivity. *Environ. Sci. Technol.* **2016**, *50* (7), 3589−3596.
(61) Wang, X.; Wang, Z.; Peak, D.; Tang, Y.; Feng, X.; Zhu, M. Quantification of coexisting inner- and outer-sphere complexation of sulfate on hematite surfaces. *ACS Earth Sp. Chem.* **2018**, *2* (4), 387−398.
(62) Baltrusaitis, J.; Schuttlefield, J. D.; Zeitler, E.; Jensen, J. H.; Grassian, V. H. Surface reactions of carbon dioxide at the adsorbed water-oxide interface. *J. Phys. Chem. C* **2007**, *111* (40), 14870−14880.
(63) Baltrusaitis, J.; Schuttlefield, J.; Zeitler, E.; Grassian, V. H. Carbon dioxide adsorption on oxide nanoparticle surfaces. *Chem. Eng. J.* **2011**, *170* (2−3), 471−481.
(64) Zheng, L.; Apps, J. A.; Spycher, N.; Birkholzer, J. T.; Kharaka, Y. K.; Thordsen, J.; Beers, S. R.; Herkelrath, W. N.; Kakouros, E.; Trautz, R. C. Geochemical modeling of changes in shallow groundwater chemistry observed during the MSU-ZERT CO2-injection experiment. *Int. J. Greenhouse Gas Control* **2012**, *7*, 202−217.
(65) Trautz, R. C.; Pugh, J. D.; Varadharajan, C.; Zheng, L.; Bianchi, M.; Nico, P. S.; Spycher, N. F.; Newell, D. L.; Esposito, R. A.; Wu, Y.; et al. Effect of dissolved CO2 on a shallow groundwater system: A controlled release field experiment. *Environ. Sci. Technol.* **2013**, *47* (1), 298−305.
(66) Tsakiroglou, C. D.; Terzi, K.; Aggelopoulos, C.; Theodoropoulou, M. CO2-induced release of copper and zinc from model soil in water. *Int. J. Greenhouse Gas Control* **2018**, *76*, 150−157.
(67) Perona, M. J.; Leckie, J. O. Proton stoichiometry for the adsorption of cations on oxide surfaces. *J. Colloid Interface Sci.* **1985**, *106* (1), 64−69.
(68) Rietra, R. P. J. J.; Hiemstra, T.; Van Riemsdijk, W. H. Electrolyte anion affinity and its effect on oxyanion adsorption on goethite. *J. Colloid Interface Sci.* **2000**, *229* (1), 199−206.
(69) Olsen, S. R.; Cole, C. V.; Watanabe, F. S.; Dean, L. A. *Estimation of available phosphorous in soils by extraction with sodium bicarbonate*; 1954.
(70) Barrow, N. J.; Shaw, T. C. Sodium bicarbonate as an extractant for soil phosphate, I. Separation of the factors affecting the amount of phosphate displaced from soil from those affecting secondary adsorption. *Geoderma* **1976**, *16* (2), 91−107.

DOI: 10.1021/acsearthspacechem.8b00160
ACS Earth Space Chem. XXXX, XXX, XXX−XXX